In-situ Synthesis and Characterization of Polyamide 6/POSS Nanocomposites

*Subramaniya Pillai Ramasundaram, Kap Jin Kim**

Summary: The nanocomposites of polyamide 6 (PA6) and polyhedral oligomeric silsesquioxane (POSS) containing primary and secondary amino groups were synthesized through in-situ polymerization. The chemical structure of the PA6/POSS nanocomposites was characterized with FT-IR and ^{1}H-NMR spectroscopies. The solution viscosity results showed the increase in intrinsic viscosity with increasing POSS loadings. The random positioning of the POSS molecules in PA6 chain was confirmed by x-ray diffraction studies. The gradual decrease in the melting point and crystallization temperature with increasing POSS content was observed by the differential scanning calorimetry. The thermogravimetric analysis results showed that the POSS incorporation does not enhance the thermal resistance of PA6/POSS nanocomposites.

Keywords: in-situ polymerization; nanocomposites; polyamide 6; POSS; solution properties

Introduction

Since polyamide 6 (PA6) is a low cost and high performance engineering thermoplastic that is known for its balance of strength, modulus, and chemical resistance, it has a potential application in the field of automobiles and other commercial products.[1,2] Hence, many research works have been carried out on PA6 to further enhance its end-use properties by means of copolymerization with other co-monomers and the incorporation of inorganic reinforcing filler materials in various dimension ranges.[3–6] Among the fillers available, the use of polyhedral oligomeric silsesquioxane (POSS) has attracted special attention because of its nanoscaled organic-inorganic hybrid structure and the availability of various functionalities which can facilitate its even distribution into organic polymer matrixes. Generally, the POSS molecules were incorporated into the polymer matrix by the conventional processing techniques such as in-situ polymerization and melt-compounding.[7–9] In recent years, POSS molecules have been successfully dispersed or incorporated in various commercial polymers.[10–13]

In the case of polyamides, the first preliminary study was reported by Iyer and Schiraldi.[14] Ricco et al. prepared the PA6-POSS nanocomposites through the hydrolytic polymerization of ε-caprolactam with aminopropyl-hepta-isobutyl POSS (AI-POSS), but a marked decrease in the molecular weight and solubility were observed with increasing POSS loading when compared with neat PA6.[15] On the other hand, an increase in molecular weight as well as appreciable improvements in the mechanical properties were observed by using heptaisobutyl-propylcarbamoylcaprolactam-POSS as an activator.[16]

In the present investigation, the PA6-POSS nanocomposites have been synthesized by in-situ ring opening polymerization of ε-caprolactam with aminoethylaminopropylisobutyl-POSS (POSS AM0275) containing both primary and secondary amino groups. The neat PA6 was also synthesized for the purpose of comparison. To the best

Department of Advanced Polymer and Fiber Materials, Kyung Hee University, Yongin, Gyeonggi-do 446-701 Korea
Fax: (+82)31 204 8114
E-mail: kjkim@khu.ac.kr

of our knowledge, no such type of POSS has been studied in PA6.

Experimental Part

Materials

Adipic acid (AA) was purchased from Lancaster. 6-aminocaproic acid (ACA), hexafluroisopropanol (HFIP), 2,2,2-trifluoroethanol (TFE), and trifluoroacetic acid (TFA) were purchased from Aldrich. Tetrahydrofuran (THF), dichloromethane (DCM), and formic acid (HCOOH) were purchased from Samchun Chemicals, Korea. ε-caprolactam (CL) from Kolon, Korea and POSS AM0275 from Hybrid Plastics were used as received.

In-situ Synthesis of PA6-POSS Nanocomposites

Mixtures of CL, ACA (initiator), POSS AM0275 (2.5 to 7.5 wt%), and AA (to maintain the stoichiometric balance between amine and carboxylic acid groups) were introduced into an autoclave at room temperature and gradually heated to 260 °C using an appropriate temperature programming. The reaction was carried out at atmospheric pressure under N_2 stream. The resultant product was extruded out in the form of spaghetti in an iced water bath and cut into small chips. The samples were Soxhlet extracted with water for 3 days in order to remove the unreacted CL, water soluble cyclic oligomers, and other low mass species.[15,17] The resultant samples were further Soxhlet extracted with THF for 3 days to remove unreacted POSS and other organic soluble species. Scheme 1 shows the overall synthesis reaction of PA6-POSS nanocomposites. The samples were coded as PA6-POSS-#.#, where #.# represents the weight percentage of POSS AM0257 fed initially.

Characterization

Fourier transform infrared (FT-IR) absorption spectra were measured using Bruker 66 V FT-IR instrument. ^{1}H-NMR spectra were recorded with a Joel JNM-AL300 (300 MHz) spectrometer using a $CDCl_3$/TFE (50/50 v/v) mixture as a solvent. Differential scanning calorimetry (DSC) was

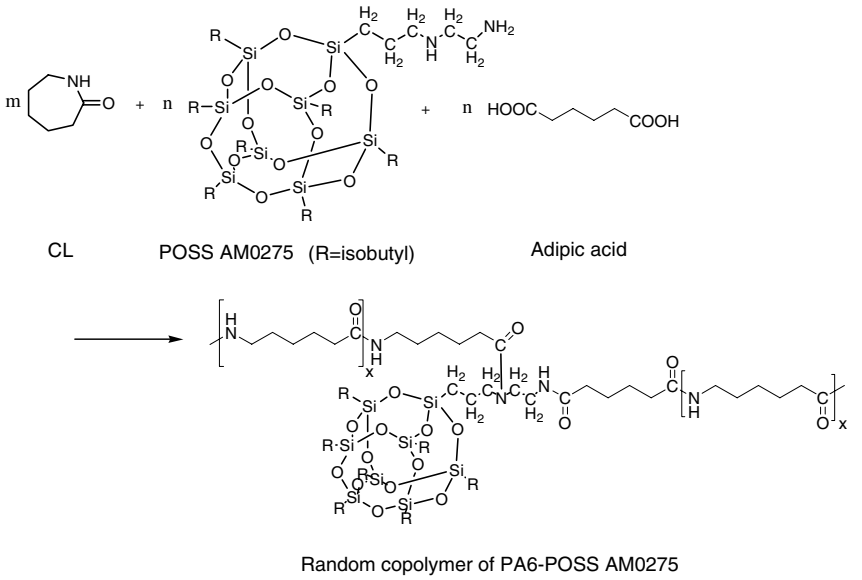

Scheme 1.
Overall synthesis reaction of PA6-POSS nanocomposites.

performed with a Thermal Analysis DSC Q1000 instrument at a scan rate of 10 °C/min. Thermogravimetric analysis (TGA) was performed with a Thermal Analysis TGA-2050 thermogravimetric analyzer at a heating rate of 10 °C/min under N_2 atmosphere in the temperature range between 25 to 600 °C. Wide angle x-ray diffraction (WAXD) patterns were obtained with Cu K_α radiation in the transmission 2D mode on a D8 DISCOVER diffractometer equipped with GADDS (Bruker AXS). The X-ray powder pattern of pure POSS AM0275 was obtained through equatorial scanning in the reflection mode with Cu K_α radiation on an MXP18 (MAC Science, POKW) diffractometer. The solution viscosity measurements were carried using a Schott AVS 260 auto viscometer with an initial sample concentration of $c = 1.5$g/dL at 20 °C using formic acid as a solvent. The solubility of the products was also assessed using different solvents.

Results and Discussion

PA6-POSS Synthesis and Characterization

In FT-IR spectra shown in Figure 1, the increasing Si–O stretching vibration peak at 1123 cm^{-1} with increasing POSS content indicates the successful incorporation of POSS AM0275 units into the PA6 main chain. The disappearance of amino group absorption at 3422 cm^{-1} (which is observed in pure POSS AM0275) also demonstrates the performance of the reaction (Figure not shown here).

Figure 2 shows the ^{1}H-NMR spectrum of purified PA6-POSS-7.5. The isobutyl moieties of the POSS AM0275 units showed three peaks at $\delta = 0.65$ [–Si–**CH$_2$**], $\delta = 1.03$ ppm [–CH–(**CH$_3$**)$_2$], and $\delta = 1.92$ ppm [–Si–CH$_2$–**CH**]. The disappearance of amino group absorption peak at $\delta = 2.0$ ppm, which is seen clearly in neat POSS, also demonstrates the incorporation of POSS into the PA6 main chain through condensation reaction. The peaks corresponding to the methylene portion of the PA6 chain was observed at the δ values of 1.32, 1.52, 1.60, 2.19, and 3.2 ppm. The mol fraction and wt.% of POSS AM0275 in the resultant nanocomposite were obtained from Eqs.(1) and (2), respectively, using the area of methylene peaks appearing in the range of 1.25∼1.75 ppm for PA6 and the area of the isobutyl peaks appearing in the range of 0.90 and 1.10 ppm for POSS. The copolymerization yield% of POSS was obtained from Eq.(3). The results are listed in Table 1 and it confirms that 58–76% of POSS fed initially was successfully incorporated into the PA6 main chain.

$$\text{mol fraction of POSS} = \frac{A_{1.03\text{ppm}}/42}{A_{1.03\text{ppm}}/42 + (A_{1.32\text{ppm}} + A_{1.52\text{ppm}} + A_{1.60\text{ppm}})/6} \quad (1)$$

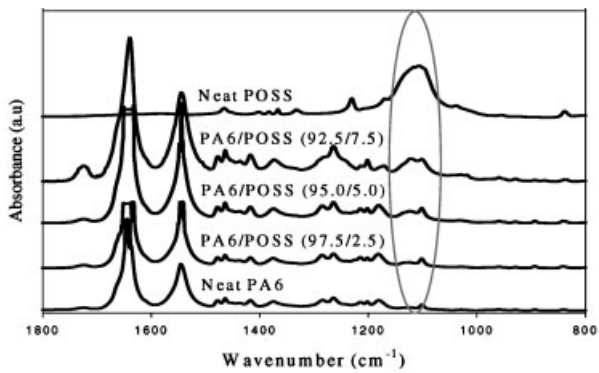

Figure 1.
FT-IR spectra of neat POSS AM0275 and purified PA6-POSS samples.

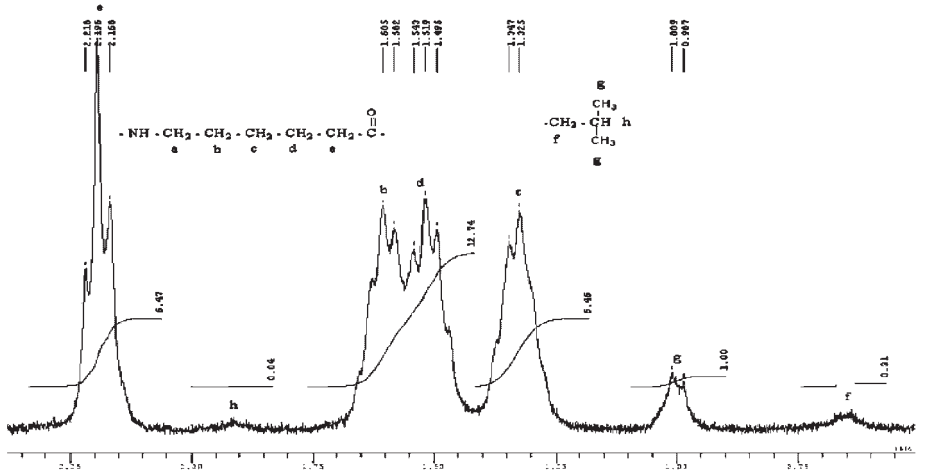

Figure 2.
^{1}H-NMR spectrum of purified PA6-POSS-7.5.

$$\text{wt.\% of POSS} = \frac{\text{mol fract. of POSS} \times \text{M.W. of POSS}}{\text{mol fract. of POSS} \times \text{M.W. of POSS} + (1 - \text{mol fract. of POSS}) \times \text{M.W. of PA6 repeating unit}} \times 100 \quad (2)$$

$$\text{yield\%} = \frac{\text{wt.\% of POSS in purified sample}}{\text{feed wt.\% of POSS}} \times 100 \quad (3)$$

Solubility and Molecular Weight

The neat PA6, PA6-POSS 2.5 and 5.0 were dissolved well in HCOOH, HFIP, and TFE, whereas medium solubility was achieved using TFA. PA6-POSS 7.5 exhibited marked decrease in the solubility for the solvents used and instead showed swelling behavior with increasing time. In order to elucidate the reason for the decreasing solubility of PA6-POSS 7.5, a binary mixture of TFE/DCM was prepared with a wide range of volume ratios. It is noted that DCM is less polar than any other solvents used above and is a good solvent for POSS AM0275. The solubility of PA6-POSS 7.5 was increased with increasing DCM content and a transparent homogeneous solution could be obtained when using 60/40 (TFE/DCM) solvent ratio. Hence, the absence of chemical cross-linking was confirmed by this solubility test. The remarkably reduced solubility of PA6-POSS 7.5 in all of the good solvents of PA6 can be correlated with the increased amount of POSS agglomerates caused by intermolecular interaction between the non-polar hydrocarbon segments of POSS

Table 1.
Composition of POSS AM0275 in the PA6-POSS and heat of fusion of PA6 part.

Sample code	Feed composition of POSS (wt. %)	POSS composition after purification (wt. %)	Yield (%)	Heat of fusion (J/g)
Neat PA6	–	–	–	53.28
PA6-POSS-2.5	2.5	1.45	58.0	47.45
PA6-POSS-5.0	5.0	3.84	76.9	45.32
PA6-POSS-7.5	7.5	5.76	76.9	42.80

based on London dispersion forces. These agglomerates of POSS copolymerized with PA6 can act as physical cross-linking sites, resulting in dramatically reduced solubility in the good solvents of PA6. Hence, a less polar solvent like DCM must be added to the polar solvents in order to obtain a homogeneous solution of PA6-POSS 7.5 through disintegration of aggregated POSS domains. When the solubility of neat POSS AM0275 was also studied with THF and molten CL, good solubility was observed in both cases. Since the homogeneous solution of POSS AM0275 is obtained in molten CL, the proposed polymerization reaction in Scheme 1 can also occur homogeneously without any aggregates of POSS AM0275 in the course of polymerization.

Based on the solubility test, intrinsic viscosity (IV) of neat PA6, purified PA6-POSS-2.5 and 5.0 were measured using HCOOH as a solvent. The IV of neat PA6 ($\eta = 1.0754$) increased to $\eta = 1.7710$ with the incorporation of 1.45 wt% POSS and slightly decreased to $\eta = 1.5515$ for 3.84 wt% of POSS. The IV of PA6-POSS-7.5 could not be measured due to its non-solubility in HCOOH. Though the magnitude of IV is related to the average molecular weight of polymer, it can be wrong to compare the average molecular weights of the homopolymer and its copolymers only with IV data, because the solution behavior of homopolymer and copolymer is sometimes not similar due to the different chain conformational statistics caused by variation in their chemical compositions. Even though the samples seem to be fully soluble in HCOOH, the presence of nanoaggregates cannot be ruled out because the HCOOH is a good solvent for PA6 units and not for POSS units. The presence of even small amount of POSS aggregates can result in high IV values due to the physical cross-linking. There is no specific reason why the addition of POSS with one primary amine and one secondary amine increases the average chain length of the resultant polymer when the polymerization is carried out with the stoichiometric balance of amine and carboxylic acid groups for the same polymerization time period. Nevertheless, the PA6-POSS nanocomposites show higher IV resulting from physical cross-linking caused by POSS aggregates in the HCOOH solution.

Crystal Structure

X-ray diffraction (XRD) scans of neat PA6 and PA6-POSS were performed before and after purification process in order to study the effect of POSS AM0275 on their crystalline structure. As shown in Figure 3(a), the X-ray diffraction scans of unpurified neat PA6 and PA6-POSS nanocomposites showed the crystalline peaks at $2\theta = 20.3^\circ$ and 23.4° which were attributed to the (200) and (002)/(202) plane

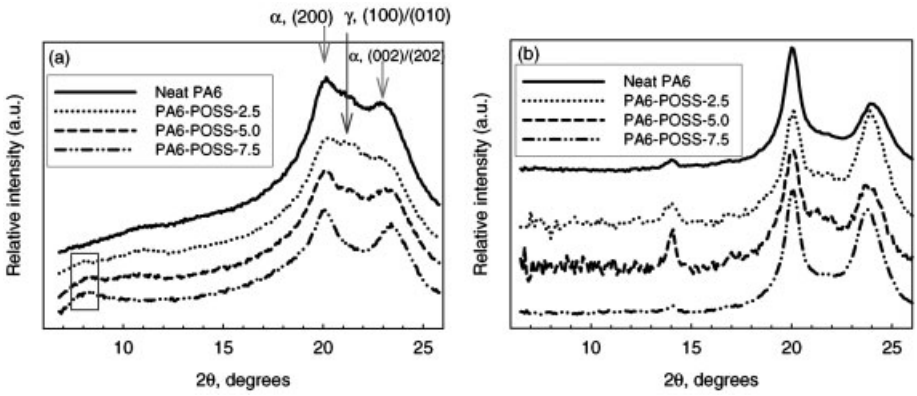

Figure 3.
X-ray diffraction patterns of PA6-POSS nanocomposites. (a) before purification; (b) after purification.

reflections of α-form, respectively. However, traces of crystalline peak could be observed around $2\theta = 21.5^\circ$ in the case of neat PA6, PA6-POSS 2.5 and 5.0, and attributed to the (100)/(010) plane reflection of the γ-form.[18,19] These results indicate that the POSS AM0275 probably plays an important role in the formation of α-crystal even at 7.5 wt.% and relatively small heterogeneous nucleation of the γ-crystal form up to 5 wt.%.[2] The broad crystalline peak associated with unreacted POSS AM0275 observed at $2\theta = 8.15^\circ$ in the unpurified PA6-POSS samples were found to increase in intensity with increasing amount of POSS content.

Figure 3(b) shows the XRD scans of purified chips of neat PA6 and PA6-POSS nanocomposites. The peak observed around $2\theta = 14^\circ$ correspond to the diffraction of adhesive tape used during sample preparation for XRD. We were able to observe two significant changes in the crystalline peaks present after purification. One is that the α-crystal peaks became much sharper and narrower and the intensity of the γ-crystal peak was reduced after purification. This change may be associated with lamella thickening caused by annealing effect, increasing crystallinity through solvent-induced crystallization and the solid-solid state transition from thermodynamically less stable γ-crystal to more stable α-crystal in the course of successive purification with hot water and THF.

The other significant change is that the diffraction peak related with the POSS AM0275 disappeared completely at $2\theta = 8.15^\circ$. This suggests that the POSS molecules incorporated into the PA6 main chain cannot form large sized aggregates to form crystalline domains. According to Ricco et al., the POSS molecules present at the end of PA6-POSS nanocomposites obtained through in-situ anionic ring opening polymerization of CL in the presence of monofunctional POSS activator showed distinct X-ray diffraction peaks.[15] Therefore the absence of POSS diffraction peak in our purified PA6-POSS samples suggests that unreacted POSS may have been removed completely during the purification process and that the POSS molecules may have located randomly in the PA6 chain.

Thermal Transition Behavior and Resistance to Thermal Degradation

As seen in Figure 4(a), the first heating scans of as-polymerized PA6 and PA6-POSS nanocomposites show the gradual depression in melting point (T_m) of crystalline PA6 domain with increasing POSS content. The random location of POSS molecules in the PA6-POSS copolymer main chain has resulted in the shorter sequence length of crystallizable PA6 leading to the formation of thinner lamella resulting in T_m depression.

In general, the appearance of either small shoulder or melting peaks prior to the main melting peak could be correlated to the presence of lamellar crystals with different structures, thickness, or crystal perfectness and they give rise to double

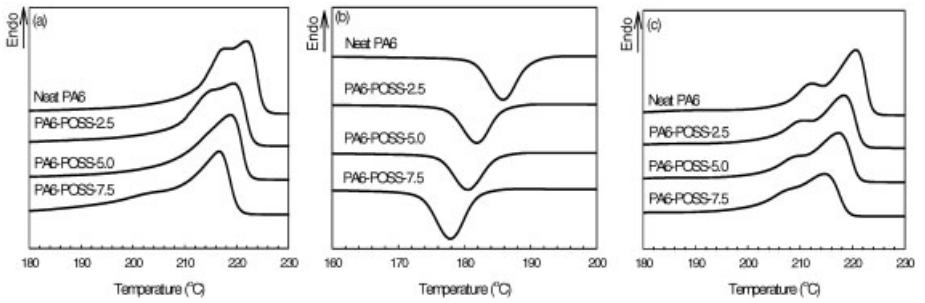

Figure 4.
DSC thermograms of as-polymerized PA6-POSS nanocomposites upon heating (a), cooling (b), and reheating (c) at the scan rate of 10 °C/min.

melting behavior via melting-recrystallization-remelting process upon heating.[20] Double melting behavior shown in Figure 4(a) can be associated with the above process and also to the co-existence of different crystal modifications α and γ as previously shown in Figure 3(a).

Figure 4(b) shows non-isothermal crystallization from the melt for PA6 and PA6-POSS. The melt-crystallization (T_{cm}) peak shifts to lower temperature with increasing feed concentration of POSS. This suggests that the incorporation of POSS in the PA6 main chain retard melt-crystallization due to the increased structural irregularity caused by random copolymerization and restricted transportation of crystallizable PA6 chain by physical cross-linking formed by the intermolecular aggregation of POSS. The second heating DSC thermogram shown in Figure 4(c) gives us information about the amount of crystalline phases formed upon cooling from the melt. Since only PA6 portion can be crystallized, we calculated the normalized heat of fusion based on the unit weight of PA6 and the results are listed in Table 1. The heat of fusion is seen to decrease with increasing POSS content, because the crystallization occurs at lower temperature and the time for complete crystallization is not permitted due to retarded melt-crystallization with increasing POSS content.

Even though samples were prepared from melt-quenching into liquid nitrogen to obtain as much amorphous phase as possible, glass transition behavior was not observed in DSC thermograms. The dynamic glass transition behavior, however, could be observed clearly in the plot of loss tan δ vs. temperature obtained from DMTA measurement as shown in Figure 5. Two significantly different relaxation peaks (labeled α and β) descending from higher to lower temperatures were observed. The α-relaxation occurring between 0∼50 °C reflects the onset motion of large chain segments caused by the breaking of molecular bridging in the amorphous region.[21] The β-relaxation at about −85 °C is caused by local segmental motion of amide groups

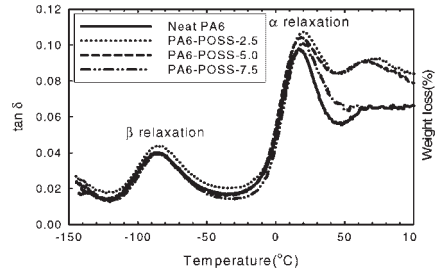

Figure 5.
Plots of tan δ versus temperature for PA6 and PA6-POSS nanocomposites.

in the amorphous region that are not hydrogen bonded to the other amide groups and several ethylene carbon groups.[21] Not as expected, however, the incorporation of POSS does not change peak temperatures of α- and β-relaxation in the POSS concentration range used in our study.

Figure 6 shows the TGA thermograms of PA6 and PA6-POSS nanocomposites. The initial weight loss was observed to occur for all the samples at around 360 °C and well pronounced in the range at 425–450 °C. Relatively similar decomposition patterns observed for both neat and POSS added PA6 indicate that POSS molecules might not be involved so much in retarding thermal degradation. The slight increase in the thermal resistance of PA6-POSS 7.5 was observed due to an increase in the SiO_x fractions in the polymer.[9]

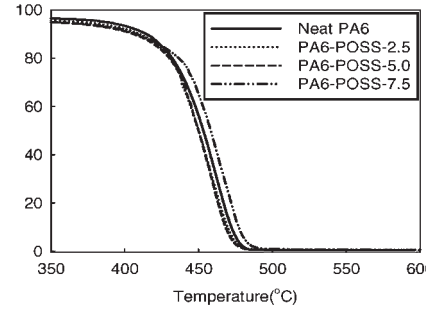

Figure 6.
TGA thermograms of PA6 and PA6-POSS nanocomposites.

Conclusions

The PA6-POSS nanocomposites with various POSS fractions were synthesized through in-situ polymerization of CL with POSS containing both primary and secondary amine groups. The incorporation of POSS molecules into the main chain of the PA6 was confirmed by both FT-IR and ^{1}H-NMR spectroscopies and the relatively high copolymerization yield of POSS was also observed by the ^{1}H-NMR spectrum. X-ray studies confirmed the random positioning of POSS in the PA6 chains. The formation of random copolymer also suggests that both amino groups of POSS have reacted with carboxylic acid groups by condensation during in-situ polymerization. The absence of chemical cross-linking in PA6-POSS 7.5 was confirmed by the solubility tests. The increase in IV of PA6-POSS was correlated with increase in the molecular weight as well as the presence of nanoaggregates of the incorporated POSS molecules. The gradual depression in the T_m and T_{cm} were observed upon heating and cooling scans on the DSC. The TGA results showed that the incorporation of POSS AM0275 does not alter resistance to the thermal degradation of the PA6.

[1] M. M. Hasan, Y. Zhou, H. Mahfuz, S. Jeelani, *Mater. Sci. Eng. A.*, **2006**, *429*, 181.
[2] Tzong-Ming Wu, Chien-Shiun Liao, *Macromol. Chem. Phys.* **2000**, *201*, 2820.
[3] T. D. Fornes, D. R. Paul, *Polymer* **2003**, *44*, 3945.
[4] Hong Ding, F. W. Harris, *Pure Appl. Chem.* **1995**, *67*, 1997.
[5] Z. Wang, Y. Zhou, P. K. Mallick, *Polym. Compos.* **2002**, *23*, 858.
[6] S. W. Shalaby, H. K. Reimschuessel, E. M. Pearce, *Polym. Eng. Sci.* **1973**, *13*, 88.
[7] Guizhi Li, L. Wang, Hanli Ni, C. U. Pittman Jr, *J. Inorg. Organomet. Polym.* **2002**, *11*, 123.
[8] M. Joshi, B. S. Butola, *J. Macromol. Sci., Polym. Rev.* **2004**, *44*, 389.
[9] Y.-L. Liu, H. C. Lee, *J. Polym. Sci., Part A: Polym. Chem.* **2006**, *44*, 4632.
[10] T. S. Haddad, B. D. Viers, S. H. Philips, *J. Inorg. Organomet. Polym.* **2001**, *11*, 155.
[11] Bruce X FU, B. S. Hsiao, H. White, M. Rafailovich, P. T. Mather, H. G. Jeon, S. Philips, J. Lichtenhan, J. Scwab, *Polym. Int.* **2000**, *49*, 437.
[12] Lie Zheng, R. J. Farris, E. B. Couhlin, *J. Appl. Polym. Sci.* **2001**, *39*, 2920.
[13] F. Gao, Y. Tong, S. R. Schriker, Dr. B. M. Culbertson, *Polym. Adv. Technol.* **2001**, *12*, 355.
[14] S. Iyer, D. Schiraldi, *Polym. Mater. Sci. Eng.* **2005**, *92*, 326.
[15] L. Ricco, S. Russo, O. Monticelli, A. Bordo, F. Bellucci, *Polymer* **2005**, *46*, 6810.
[16] F. Baldi, F. Bibnotti, L. Ricco, O. Montecelli, T. Ricco, *J. Appl. Polym. Sci.* **2006**, *100*, 3409.
[17] Ch. A. Kruissink, G. M. Van der Want, A. J. Staverman, *J. Polym. Sci.* **1958**, *30*, 67.
[18] D. P. Russel, P. W. R. Beaumont, *J. Mater. Sci.* **1980**, *15*, 197.
[19] J. P. Parker, P. H. Lindermeyer, *J. Appl. Polym. Sci.* **1977**, *21*, 821.
[20] N. Song, D. Yao, Z. Y. Wang, P. R. Sundararajan, *Polymer* **2005**, *46*, 3831.
[21] S. Ghosh, D. Khastgir, A. K. Bhowmick, *Polymer* **1998**, *39*, 3967.

